Optical modulation of continuous terahertz waves towards cost-effective reconfigurable quasi-optical terahertz components

Li-Jing Cheng[1] and Lei Liu[2,*]

[1]*School of Electrical Engineering and Computer Science, Oregon State University, OR 97311, USA*
[2]*Department of Editorial Engineering, University of Notre Dame, IN 46556, USA*
[*]*lliu3@nd.edu*

Abstract: We report optical modulation of continuous terahertz (THz) wave in the frequency range of 570-600 GHz using photo-induced reconfigurable patterns on a silicon wafer. The patterns were implemented using programmable illumination from a commercially-available digital light processing (DLP) projector. A modulation depth of 20 dB at 585 GHz has been demonstrated. Modulation speed measurement shows a 3-dB bandwidth of ~1.3 kHz which is primarily limited by the DLP system. A photo-induced polarizer with tunable polarization angle has been demonstrated, showing a 3-dB extinction ratio. Reconfigurable aperture-arrays (4 x 4 pixels) have been attempted for room-temperature coded-aperture imaging using a single Schottky diode detector at 585 GHz. We envision that this technique will provide a simple but powerful means to realize a variety of cost-effective reconfigurable quasi-optical THz circuits and components.

OCIS codes: (130.1750) Components; (040.2235) Far infrared or terahertz; (230.4110) Modulators; (170.6795) Terahertz imaging.

References and links

1. W. L. Chan, H.-T. Chen, A. J. Taylor, I. Brener, M. J. Cich, and D. M. Mittleman, "A spatial light modulator for terahertz beams," Appl. Phys. Lett. **94**(21), 213511 (2009).
2. H.-T. Chen, W. J. Padilla, J. M. O. Zide, A. C. Gossard, A. J. Taylor, and R. D. Averitt, "Active terahertz metamaterial devices," Nature **444**(7119), 597–600 (2006).
3. H.-T. Chen, S. Palit, T. Tyler, C. M. Bingham, J. M. O. Zide, J. F. O'Hara, D. R. Smith, A. C. Gossard, R. D. Averitt, W. J. Padilla, N. M. Jokerst, and A. J. Taylor, "Hybrid metamaterials enable fast electrical modulation of freely propagating terahertz waves," Appl. Phys. Lett. **93**(9), 091117 (2008).
4. H.-T. Chen, W. J. Padilla, M. J. Cich, A. K. Azad, R. D. Averitt, and A. J. Taylor, "A metamaterial solid-state terahertz phase modulator," Nat. Photonics **3**(3), 148–151 (2009).
5. O. Paul, C. Imhof, B. Lägel, S. Wolff, J. Heinrich, S. Höfling, A. Forchel, R. Zengerle, R. Beigang, and M. Rahm, "Polarization-independent active metamaterial for high-frequency terahertz modulation," Opt. Express **17**(2), 819–827 (2009).
6. C.-Y. Chen, C.-L. Pan, C.-F. Hsieh, Y.-F. Lin, and R.-P. Pan, "Liquid-crystal-based terahertz tunable Lyot filter," Appl. Phys. Lett. **88**(10), 101107 (2006).
7. B. Sensale-Rodriguez, R. Yan, M. M. Kelly, T. Fang, K. Tahy, W. S. Hwang, D. Jena, L. Liu, and H. G. Xing, "Broadband graphene terahertz modulators enabled by intraband transitions," Nat Commun **3**, 780 (2012).
8. B. Sensale-Rodriguez, S. Rafique, R. Yan, M. Zhu, V. Protasenko, D. Jena, L. Liu, and H. G. Xing, "Terahertz imaging employing graphene modulator arrays," Opt. Express **21**(2), 2324–2330 (2013).
9. J. Wu, B. Jin, Y. Xue, C. Zhang, H. Dai, L. Zhang, C. Cao, L. Kang, W. Xu, J. Chen, and P. Wu, "Tuning of superconducting niobium nitride terahertz metamaterials," Opt. Express **19**(13), 12021–12026 (2011).
10. H. Alius and G. Dodel, "Amplitude-, phase-, and frequency modulation of far-infrared radiation by optical excitation of silicon," Infrared Phys. **32**, 1–11 (1991).
11. T. Vogel, G. Dodel, E. Holzhauer, H. Salzmann, and A. Theurer, "High-speed switching of far-infrared radiation by photoionization in a semiconductor," Appl. Opt. **31**(3), 329–337 (1992).
12. S. F. Busch, S. Schumann, C. Jansen, M. Scheller, M. Koch, and B. M. Fischer, "Optically gated tunable terahertz filters," Appl. Phys. Lett. **100**(26), 261109 (2012).

#198504 - $15.00 USD Received 30 Sep 2013; accepted 5 Nov 2013; published 14 Nov 2013

13. S. Busch, B. Scherger, M. Scheller, and M. Koch, "Optically controlled terahertz beam steering and imaging," Opt. Lett. **37**(8), 1391–1393 (2012).
14. D. Shrekenhamer, C. M. Watts, and W. J. Padilla, "Terahertz single pixel imaging with an optically controlled dynamic spatial light modulator," Opt. Express **21**(10), 12507–12518 (2013).
15. L. Liu, Q. Xiao, H. Xu, J. C. Schultz, A. W. Lichtenberger, and R. M. Weikle, "Design, fabrication and characterization of a submillimeter-wave niobium HEB mixer imaging array based on the 'reversed-microscope' concept," IEEE Trans. Appl. Supercond. **17**(2), 407–411 (2007).
16. N. W. Ashcroft and N. D. Mermin, *Solid State Physics* (Saunders College Publishing, 1976).
17. R. Ulbricht, E. Hendry, J. Shan, T. F. Heinz, and M. Bonn, "Carrier dynamics in semiconductors studied with time-resolved terahertz spectroscopy," Rev. Mod. Phys. **83**(2), 543–586 (2011).
18. L. Fekete, J. Y. Hlinka, E. Kadlec, P. Kuzel, and P. Mounaix, "Active optical control of the terahertz reflectivity of high-resistivity semiconductors," Opt. Lett. **30**(15), 1992–1994 (2005).
19. A. Das, C. Megaridis, L. Liu, T. Wang, and A. Biswas, "Design and synthesis of superhydrophobic carbon nanofiber composite coatings for terahertz shielding and attenuation," Appl. Phys. Lett. **98**(17), 174101 (2011).
20. L. Liu, R. Pathak, L.-J. Cheng, and T. Wang, "Real-time frequency-domain terahertz sensing and imaging of isopropyl alcohol-water mixtures on a microfluidic chip," Sens. Actuators B Chem. **184**, 228–234 (2013).
21. L. Liu, J. Hesler, H. Xu, A. Lichtenberger, and R. Weikle, "A broadband quasi-optical terahertz detector utilizing a zero bias schottky diode," IEEE Microw. Wirel. Compon. Lett. **20**(9), 504–506 (2010).
22. P. F. Goldsmith, *Quasioptical Systems: Gaussian Beam Quasi-Optical Propagation and Applications* (Wiley & Sons, Inc. 1997).
23. C. M. Li, T. Sjodin, and H. L. Dai, "Photoexcited carrier diffusion near a Si-111 surface: Non-negligible consequence of carrier-carrier scattering," Phys. Rev. B **56**(23), 15252–15255 (1997).
24. L. Zhang, J. H. Teng, H. Tanoto, S. Y. Yew, L. Y. Deng, and S. J. Chua, "Terahertz wire-grid polarizer by nanoimprinting lithography on high resistivity silicon substrate," The International Conference on Infrared, Millimeter, and Terahertz Waves, Rome, Italy (2010).
25. I. Yamada, K. Takano, M. Hangyo, M. Saito, and W. Watanabe, "Terahertz wire-grid polarizers with micrometer-pitch Al gratings," Opt. Lett. **34**(3), 274–276 (2009).
26. L. Ren, C. L. Pint, L. G. Booshehri, W. D. Rice, X. Wang, D. J. Hilton, K. Takeya, I. Kawayama, M. Tonouchi, R. H. Hauge, and J. Kono, "Carbon Nanotube Terahertz Polarizer," Nano Lett. **9**(7), 2610–2613 (2009).
27. E. Hecht, *Optics* (Addison-Wesley, 2001).
28. L. Liu, H. Xu, A. W. Lichtenberger, and R. M. Weikle, "Integrated 585 GHz hot- electron mixer focal-plane arrays based on annular-slot antennas for imaging applications," IEEE Trans. Microw. Theory Tech. **58**(7), 1943–1951 (2010).
29. S. Hawasli, N. Alijabarri, and R. M. Weikle II, "Schottky diode arrays for submillimeter-wave sideband generation," 37th International Conference on Infrared, Millimeter, and Terahertz Waves, Wollongong, NSW, Australia, (2012).
30. I. Valova and Y. Kosugi, "Hadamard-based image decomposition and compression," IEEE Trans. Inf. Technol. Biomed. **4**(4), 306–319 (2000).
31. W. L. Chan, K. Charan, D. Takhar, K. F. Kelly, R. G. Baraniuk, and D. M. Mittleman, "A single-pixel terahertz imaging system based on compressed sensing," Appl. Phys. Lett. **93**(12), 121105 (2008).
32. A. Kannegulla, Z. Jiang, S. Rahman, P. Fay, H. G. Xing, L.-J. Cheng, and L. Liu, "Coded-aperture imaging using photo-induced reconfigurable aperture arrays for mapping terahertz beams," IEEE Trans. Terahertz Sci. Technol. (submitted to).

1. Introduction

Recently, terahertz (THz) waves have attracted increased attention and interest owning to their prospective applications in many important fields, such as astronomy, chemical analysis, biological sensing, imaging and security screening. Much effort has been devoted to developing THz sources and detectors, which has turned THz research into a rapidly growing technological field. However, the research into active components for manipulation and modulation of THz radiation is still in its infancy. One of the key components mostly desired for advanced THz circuits and systems is a tunable/reconfigurable quasi-optical THz device that actively controls the spatial transmission of an incident THz wave. This kind of devices enables us to implement various functions (e.g., THz wave switching, attenuating, focusing and steering) and encode information on THz waves. Such functional THz devices are still scarce but in high demand for sophisticated circuits and systems needed in THz sensing, imaging and communication.

Demonstrations of the above active THz circuits and components have been reported using metamaterials [1–5] liquid-crystal-based devices [6], graphene modulator arrays [7, 8] and thermal-sensitive elements [9]. However, most of them relied on prepatterned metal

#198504 - $15.00 USD Received 30 Sep 2013; accepted 5 Nov 2013; published 14 Nov 2013

electrodes to produce multipixel arrays, which greatly limits the achievable tunability and versatility. An alternative means of tuning and modulating THz wave is based on optically induced free carriers in semiconductors [10, 11]. Relatively weak modulations (e.g., ~75% modulation depth) of far-infrared (FIR) radiation were demonstrated using silicon wafers illuminated by laser beams [10]. THz all-optical tunable filters, beam-steering gratings and imaging devices have been demonstrated using photo-induced patterns on semiconductor materials [12–14]. However, experiments performed so far were primarily focused on time-domain using pulsed THz waves and the modulation depth and speed have not yet been systematically studied [12, 13].

Owning to the significant development in continuous-wave (CW) THz sources (e.g., quantum cascade lasers), detectors, and other circuits and components (e.g. THz amplifiers) over the past decade, a variety of frequency-domain THz measurement and characterization systems including THz spectroscopy and vector-network analyzer (VNA) have been demonstrated and become commercially available. Compared to time-domain techniques, CW THz systems feature higher average beam power, higher spectral resolution and faster data acquisition. In order to apply the photo-excitation technique to realize practical THz quasi-optical components for operating in CW THz systems, important parameters in the CW mode (e.g., modulation depth and speed) must be systematically studied. In addition, although THz quasi-optical components have been greatly developed in the last decade and are widely utilized in THz systems, most of them have fixed THz response, and have proven extremely costly to manufacture and fabricate (e.g. thousands of US dollars per filter or polarizer). Cost-effective and reconfigurable THz quasi-optical components are then highly demanded.

In this letter we study optical modulation of continuous THz waves in the frequency range of 570-600 GHz using programmable illumination patterns mapped on a semi-insulating silicon wafer by a commercially available digital light processing (DLP) projector (instead of using laser beams as reported in [14]). A 20 dB modulation depth and ~1.3 KHz modulation speed have been measured at 585 GHz. We further demonstrate a reconfigurable quasi-optical THz polarizer with tunable polarization angle. Reconfigurable aperture-arrays (4 x 4 pixels) have also been attempted for room-temperature coded-aperture imaging (CAI) using a single Schottky diode detector at 585 GHz. The reconfigurability of the above components was realized by projecting computer-generated photopatterns on the silicon wafer using the low-cost DLP projector. This approach is relative simple, powerful and cost-effective for creating unlimited possibilities of reconfigurable quasi-optical THz components that are highly desired in THz sensing, imaging and communication.

2. Theory

Semi-insulating silicon wafers in their steady state are quite transparent to THz radiation with a low insertion loss in the range of ~2dB/cm [15]. However, when they are under photoexcitation, free carriers can be generated within the penetration depth forming a layer of electron plasma that interacts with THz radiation. The strength of the interaction between THz radiation and the photo-excited carriers in a semiconductor can be adjusted by the intensity of illumination.

#198504 - $15.00 USD Received 30 Sep 2013; accepted 5 Nov 2013; published 14 Nov 2013

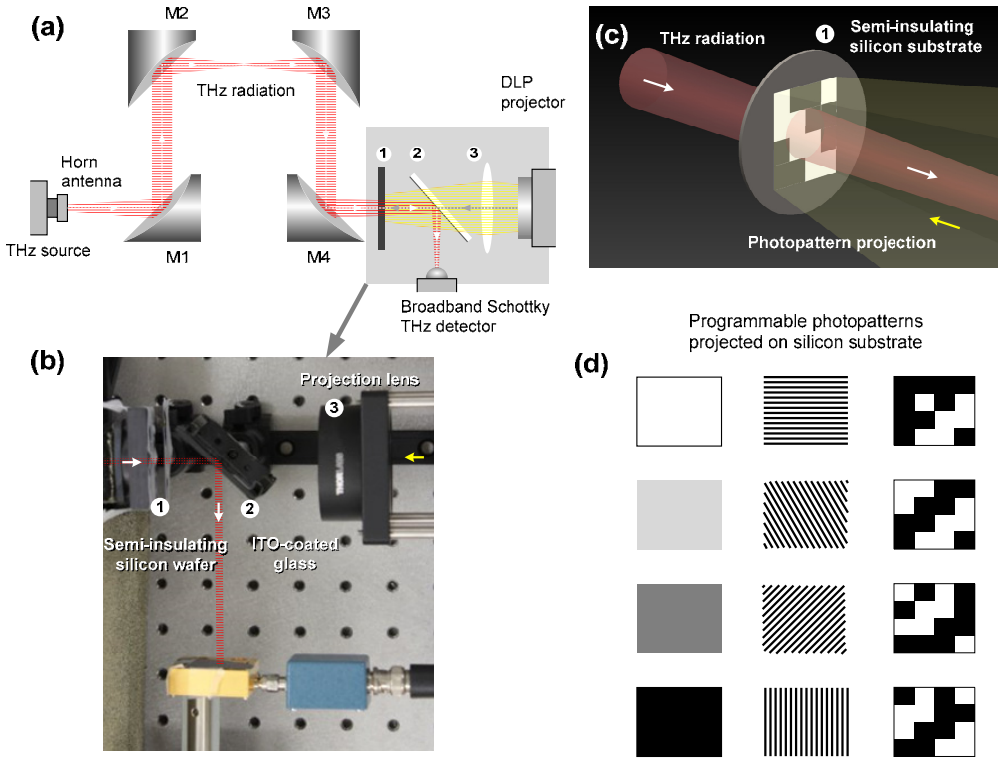

Fig. 1. (a) Experimental setup for CW THz modulation and reconfigurable THz quasi-optical component using photo-induced pattern on semi-insulating silicon. (b) Highlight image of the modulator setup. (c) Render of the key component in the proposed system that enables reconfigurable THz modulation. DLP projector generates reconfigurable conductive patterns on the silicon to interact with the incident THz beam. (d) Modulation types demonstrated in this work. Left column: unpatterned gray scales for THz intensity modulation; middle column: patterns for reconfigurable THz polarizer; and right column: exemplary reconfigurable aperture array patterns for potential THz coded aperture imaging.

In detail, when light illuminates on a semiconductor material, free carriers composed by electrons and holes may be generated as long as the energy of light surpasses the band gap energy of the semiconductor. These photoexcited carriers survive for a scattering time τ, before they are annihilated by recombination and thereby contribute to photoconductivity of the semiconductor material. The complex conductivity of the semiconductor can be expressed by the Drude response $\sigma_D(\omega) = \epsilon_0 (\omega_p^2 \tau) / (1 - i\omega\tau)$, which is characterized by a Lorentzian resonance centered at zero frequency with a linewidth τ^{-1}, i.e., the inverse of the carrier scattering time. The amplitude of the Drude conductivity response is determined by the plasma frequency ω_p, defined as $\omega_p^2 = ne^2 / (\epsilon_0 m^*)$, with n being the mobile charge carrier density, ε_0 the permittivity of free space, τ the scattering time, m^* the effective mass contributed by both electron (m_e) and hole (m_h) following a relation $1/m^* = 1/m_e + 1/m_h$ and e the electron charge [16, 17]. Photoexcitation generates equal amount of electrons and holes and the carrier density n is determined by the energy density of the incident photons [18]. The expression indicates that by tuning the plasma frequency ω_p with varied extension of photoexcitation, it is possible to adjust the opacity of semiconductor materials to the electromagnetic radiation of a certain frequency—below ω_p the material behaves metallic and is opaque to the THz wave whereas above ω_p it becomes dielectric and transparent. This phenomenon can be applied to modulate THz wave and generate reconfigurable quasi-optical THz circuits and components directly on silicon wafer.

#198504 - $15.00 USD Received 30 Sep 2013; accepted 5 Nov 2013; published 14 Nov 2013

3. Experiment

The experimental setup as shown in Fig. 1(a) was implemented by integrating a frequency-domain THz spectrometer (THz-FDS) system [19, 20] and a photo-induced modulator which utilized a DLP system to create programmable conductive patterns on a semi-insulating silicon wafer (undoped, resistivity >20,000 Ω-cm) for THz wave modulation. A frequency extension module (FEM, Virginia Diodes, Charlottesville, VA), comprised by a series of nonlinear Schottky diode frequency multipliers (i.e. three doublers D55v2, D100v3 and D200 as well as a WR-1.5 tripler) and a WR-1.5 horn antenna, serves as the THz source in the frequency range of 570–630 GHz with an output power of ~1mW. A 0.05–20 GHz phase-locked microwave sweep oscillator (E8247 C, Agilent, Santa Clara, CA) and a power amplifier (A246-2XW-31, Spacek Labs, Santa Barbara, CA) with a built-in doubler were used for the signal input. The THz detector was developed using a zero-bias Schottky diode (ZBD) and a lens-coupled sinuous antenna for ultra-broadband operation in the frequency range of 0.1–1 THz [21]. The measured average detector responsivity is ~500 V/W, and the noise equivalent power (NEP) is 5–20 pW/√Hz. To ensure square-law detection, the output signal level from this detector for all measurement in this paper was controlled to be less than 20 mV. The THz beam was collimated and focused twice through two sets of off-axis parabolic mirrors M1/M2 and then M3/M4 before it was focused onto the detector. Between the mirror M4 and the detector, a 200 μm thick double side polished semi-insulating silicon wafer was placed followed by an indium tin oxide (ITO) coated glass plate. The ITO plate was mounted at 45 degree as respect to the path of both incident THz beam and the photo-excitation light, functioning as a beam combiner/splitter, which is transparent to visible light while reflecting THz wave.

The illumination patterns were created by a modified commercially available digital micromirror device (DMD)-based DLP projector. The modified DLP system contained an original 0.7" DMD panel with 1024 x 768 dot resolution and a 200 W mercury lamp. The RGB filter wheel was removed to allow generating white light images with a maximum brightness of ~2500 lumens after passing through a visible bandpass filter (400 - 800 nm). The projection optics was redesigned to focus the image down to an area of 12 mm x 9 mm with a working distance of 120 mm.

The modulator setup is highlighted in Fig. 1(b) in which the horizontally-polarized continuous THz beam was focused by mirror M4, passed through the silicon wafer and then reflected 90 degrees by the ITO plate toward the THz detector. The THz detector had a linear polarization and was oriented to sense the horizontally-polarized portion of the THz beam. A Labview program was engaged to real-time monitor the output voltage from the detector. The key function that enables reconfigurable THz modulation is rendered in Fig. 1(c) in which a DLP system is utilized to generate photoconductive patterns on a silicon substrate to manipulate the transmitted THz wave. As illustrated in Fig. 1(d), several types of modulations were demonstrated using various photo-excited patterns on the silicon substrate, including uniform light with different gray-scale intensities, linear wire-grid with varied orientations and a 4 x 4 reconfigurable aperture array. These illumination patterns were created to implement THz intensity modulation, tunable THz polarizer and reconfigurable aperture arrays for room-temperature THz coded-aperture imaging (CAI), respectively.

#198504 - $15.00 USD Received 30 Sep 2013; accepted 5 Nov 2013; published 14 Nov 2013

4. Results and discussion

4.1 Continuous THz wave modulation

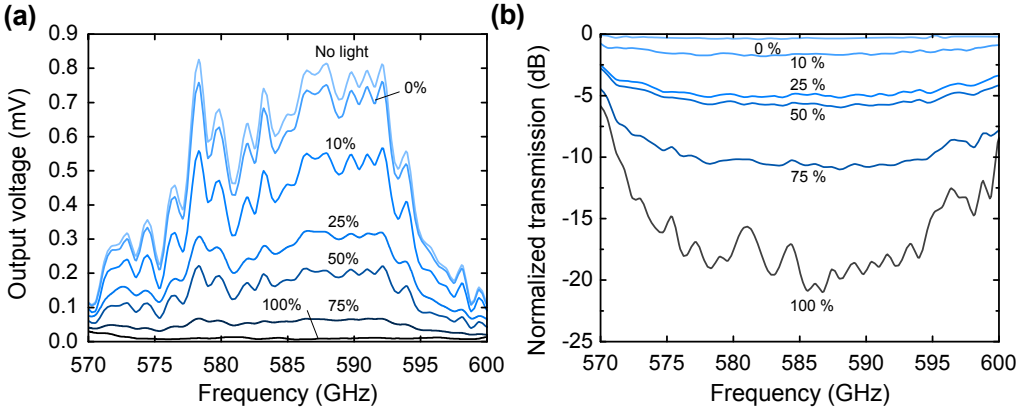

Fig. 2. Results for continuous THz wave modulation: (a) measured THz responses with various intensities of photoexcitation from no light to 100% (~2W/cm^2), and (b) normalized transmission showing a modulation depth of 20 dB at 585 GHz for white light (100%).

As discussed in the previous sections, semiconductors may generate free carriers under photoexcitation thus changing the conductivity, and hence the THz transmission. To verify the THz modulation, we generated unpatterned, uniform light with different gray scales (as seen in Fig. 1(c)) from the DLP projector. This light was illuminated (focused) onto the 200 μm thick semi-insulating silicon in an area of 12 × 9 mm^2 which was designed to cover the entire focused THz beam (~8 mm in diameter) at this position based on Gaussian optics calculation [22]. The spectrum measurement indicated that most of the light radiation from the DLP system was in the wavelength range between 530 nm and 650 nm with the strongest intensity around 550 nm, and the projection light intensity, P_{ex}, was estimated to be ~2 W/cm^2. The absorption coefficient α and reflectivity R of silicon at 550 nm are 6.4 × 10^3 cm^{-1} and 0.37, respectively. The large absorption coefficient implies a short penetration depth of about 1.5 μm. The photoinduced carrier density n_{ph} is estimated to be in the order of 10^{17} cm^{-3} using the relation $n_{ph} = \tau G_p$, with the carrier lifetime τ being ~1 μs and the generation rate $G_p = \alpha P_{ex} (1\text{-}R)/(h\nu\, q)$ where q is the electron charge and $h\nu$ = 2.25 eV for 550 nm light. The excited carrier density yields a corresponding plasma frequency of about 3 THz at silicon surface, implying that the illuminated area is opaque to the THz wave (570-600 GHz) exploited in the experiment.

The light intensity of the DLP illumination was expressed as an 8-bit grayscale (256 gray levels). To facilitate interpretation of the measures, we employ percentages to define the light intensity, viz. 0% as the weakest intensity (0 grayscale or black) and 100% as the strongest intensity of light (255 grayscale or white) giving a measured intensity of ~2W/cm^2. With the light intensity of DLP illumination increased from 0% (black) to 100% (white), the THz response was monitored by recording the output voltage of the Schottky detector. Figure 2(a) shows the measured transmission spectrum over the frequency range of 570-600 GHz responding to different light intensities ranging from 0% to 100% and off (no light). It is clearly seen that with increasing of photo-excitation intensity, the number of free carrier increases resulting in reduced transmitted THz power (power proportional to voltage in square-law region of the detector). Figure 2(b) shows the normalized THz transmission or the THz transmittance (in decibels) of the photo-excited silicon wafer. All data were normalized to the THz response measured with no illumination (P_0). The transmittance here is defined by T (dB) = $-10 \log_{10}(P/P_0)$, where P is transmitted THz power with photo-excitation. The transmittance curves for lower intensities (< 50%) in Fig. 2(b) are quite uniform over the

#198504 - $15.00 USD Received 30 Sep 2013; accepted 5 Nov 2013; published 14 Nov 2013

entire frequency range. The nonuniformities observed (e.g., the dip at ~585 GHz) for the highest intensity curve (100%) were generated by reduced measurement system dynamic range due to the specific THz source and detector employed in this experiment (see Fig. 1(a), lower response at both ends of this frequency range 570-600 GHz). In addition, the 200 μm thick silicon employed in this experiment introduced a standing wave with nearly 500 GHz period to the measurement spectra. This period is much larger than the 30 GHz measurement frequency band, so the standing wave effect by the silicon wafer has minor influence to the measurement. This minor influence can be effectively removed from the original data by normalization since the dielectric constant and thickness of the silicon wafer did not change during the experiment. At the center of the measurement frequency band, a modulation depth as large as 20 dB was measured at 585 GHz demonstrating that the white light from this projector can be used to effectively "block" or modulate the THz radiation in this frequency band. Although a relatively low-cost DLP projector was used in this experiment, much improved modulation depth was demonstrated as compared to those reported [10].

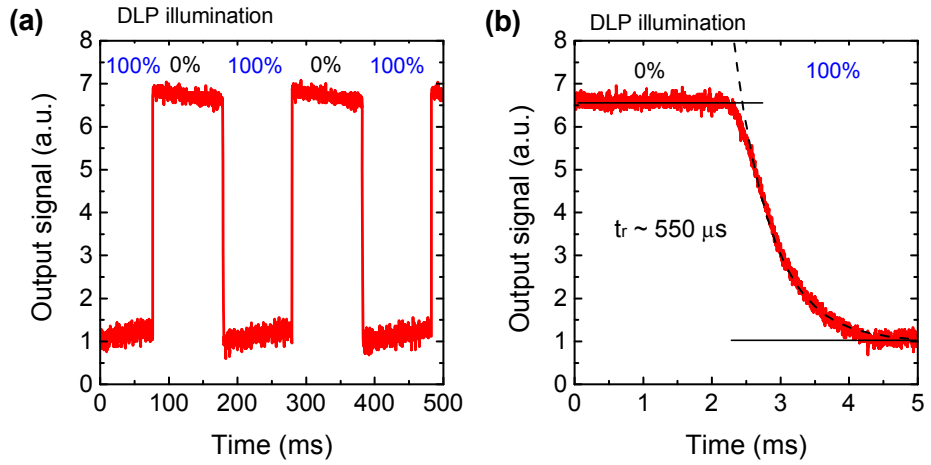

Fig. 3. (a) Time response of photoinduced THz wave modulation (585 GHz) by switching DLP projection light at 5 Hz. (b) A zoom-in view of a pulse transition. The transition time was determined by the switching rate of the DMD panel and was measured to be ~550 μs.

To estimate the photoinduced continuous wave THz modulation speed, we illuminated uniform white light pulses (255 grayscale or 100% radiation defined in this paper) separated by black light (0%) to the silicon substrate at a frequency of 5 Hz. Figure 3(a) shows the modulated THz output signals (585 GHz) corresponding to the photo-excitation from the DLP. As expected, white light (or 100% intensity) turned the silicon wafer more conductive and therefore "block" the THz transmission, while black light (or 0% intensity) illumination gave higher THz response. The transient response of the temporal THz modulation was enlarged and shown in Fig. 3(b). The 10-90% roll-off time is estimated to be ~550 μs, corresponding to a 3-dB bandwidth of ~1.3 KHz. This modulation speed is much slower than what is expected based on the free carrier recombination rate in silicon [10] and is indeed limited by the switching rate of the DMD array in the DLP projector. The observed switching time is much longer than the carrier lifetime τ ~1 μs and the diffusion time $\delta^2/4D$ ~0.5 ns where $\delta = \alpha^{-1}$ = 1.5 μm is the absorption depth and D the self-diffusion coefficient of the excited carriers [23]. This modulation speed is rather limited by the speed of the DMD array control electronics (~1.9 kHz) in the DLP projector. Upon frame switching the micromirrors switch line-by-line sequentially over the entire array with each pixel flipping responding to capacitive charging. The scanning methods plus the electronic system cause the slow transient time (hundred microseconds) much longer than the carrier lifetime (microsecond). High speed

#198504 - $15.00 USD Received 30 Sep 2013; accepted 5 Nov 2013; published 14 Nov 2013

DMD chipsets such as DLPC 410 by Texas Instruments, Inc. could be employed to provide a 32 kHz frame rate for much improved modulation speed. In spite of DMD's relatively slower transient rate, its capability of generating programmable conductive patterns to interact with THz wave provides a simple, versatile and cost-effective approach to realize reconfigurable spatial THz wave modulation and manipulation that other techniques can hardly achieve.

4.2 Photo-induced reconfigurable THz polarizers

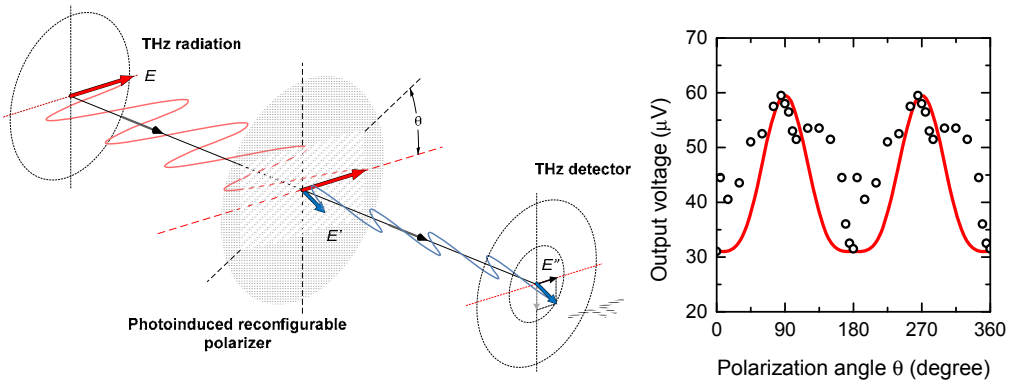

Fig. 4. (a) A THz polarizer oriented with an angle θ as respect to the E-field of the incident THz wave. In this experiment, a linear polarized detector aligned to the incident E-field was employed. (b) Measured THz response (585 GHz) versus polarization angle (empty circles) showing a ~3 dB extinction ratio. The THz wave transmits through a polarizer and is then captured by a linearly polarized detector; thus overall it experiences linear polarization twice. The detected THz energy follows a fitting curve (solid red curve) proportional to $\sin^4\theta$ predicted based on Malus' Law [26].

In order to demonstrate the capability of the optical modulation approach for generating reconfigurable THz quasi-optical components, we present the use of bi-tonal wire-grid pattern illuminated on the silicon wafer to create tunable THz polarizers. Ideal THz polarizers, as shown in Fig. 4(a) are highly anisotropic devices that present maximum transmission ($T_\perp$) with incident wave polarization perpendicular to the alignment axis, while having highest attenuation ($T_{//}$) with polarization parallel to the alignment direction. Typical THz polarizers usually consist of well-aligned conductive metal wire-grids with their pitch size much less than one wavelength. On the basis of the results in the previous sections, the wire-grid patterns could be directly generated optically onto the silicon wafer to form polarizers without any microfabrication processes such as nanoimprinting, lithography and chemical etching [24–26]. In addition, the patterns can be modified and reconfigured optically in a high speed leading to many potential novel applications. For a prototype demonstration, the wire-grid patterns in this experiment were produced using black and white (bi-tonal) images with a 30% duty cycle and an estimated density of approximately 150 lines cm^{-1}. This resulted in a strip width of ~45 μm and a pitch size of ~45 μm which is much smaller than the THz wavelengths in the frequency range of 570-600 GHz (~500 μm in free space and ~150 μm in silicon). The orientation (measured by the polarization angle between the wire-grid alignment direction and the THz source E-field direction,θ) of the wire-grid pattern was reconfigured by generating rotated images using the DLP. As shown in Fig. 4(b), the measured THz response at 585 GHz from the detector (proportional to transmitted power) versus the polarization angle is plotted using empty circles. As expected, minimum THz power transmission was measured for parallel orientation (θ = 0°) and maximum attenuation observed for perpendicular orientation (θ = 90°). The extinction ration ($T_\perp$/ $T_{//}$) is estimated to be ~3 dB. It is also seen that the transmitted THz power (or the output voltage), which passed through the photo-induced polarizer and was then received by the horizontally polarized detector, follows the fitting curve (solid red curve) proportional to $\sin^4\theta$. Based on the Malus' Law [27], the relation is

#198504 - $15.00 USD Received 30 Sep 2013; accepted 5 Nov 2013; published 14 Nov 2013

acquired given the fact that the polarization takes place twice throughout the system—first through the polarizer and then the linearly polarized detector as depicted in Fig. 4(a). The result shows that photo-induced reconfigurable THz polarizer worked reasonably well. An extinction ratio as high as ~8 dB has been achieved using this approach in a separate experiment with optimized optics. Several factors limited the polarization performance when the DLP induced photopatterns are used. For instance, the density of the wire-grid is limited by the resolution of the DLP system and the inevitable aliasing in all these digital images, especially when the wire-grid is not horizontally and vertically oriented. In addition, since the light source is not coherent and monochromatic, the projected wire-grid images tend to disperse and can hardly acquire high-contrast patterns. It is believed that the photo-induced polarizer performance could be further improved by generating finer grid patterns with better contrast.

4.3 Reconfigurable aperture arrays for cost-effective and room-temperature THz coded-aperture imaging

Compared to THz imaging using mechanical scanning and focal-plane arrays [28], CAI with aperture array masks offers the advantage of both high performance (e.g., high signal-to-noise ratio and high imaging speed) and simple and low-cost systems. In this imaging technique, single THz detector in combination with a series of N x N coded aperture masks is required for an image with an N x N resolution. N^2 measurements are performed and the same number of linear equations are then solved to reconstruct the object image. In order to achieve high-speed THz CAI, aperture arrays electronically actuated by Schottky varactor diodes [29] and graphene modulators [7, 8], respectively, have been proposed to realize such masks. Once again, all the above approaches require complicated and prepatterned circuits and wires for operation, which results in expensive and complex systems especially for large-scale, high-resolution imaging. For example, a 100 x 100 pixel imaging requires 10000 diodes for antennas or same amount of contacts for graphene modulators. The optical modulation mechanism presented in this paper could be potentially applied to generate extremely large-scale coded masks (e.g., 1024 x 768, only limited by the resolution of the DLP projector and carrier diffusion lengths in the Si wafer) for CAI without increasing the cost at all.

Although similar CAI technique has been reported in [14] using laser beams and a cooled silicon bolometer with integration over a broad frequency range. We demonstrate room-temperature CAI using the photo-induced reconfigurable aperture arrays (Fig. 1(c), directly illuminated by a commercial DLP) and a single Schottky diode detector [21] at 585 GHz. This approach may pave the way for realizing compact, low-cost THz cameras for many applications. For prototype demonstration, we performed THz imaging with 4 x 4 pixel arrays (16 arrays, each with 16 photo-induced apertures). We employed a simplest coding in which only one aperture is turned off (photo-excited) for each array. A more sophisticated coding such as Haddmad coding [30] or compressed coding [31] could be adopt for much improved performance. The measurement was performed automatically with a LabView program. Each array pattern was illuminated onto the silicon wafer for two seconds (ON-state), followed by a full black image for another 2 seconds (OFF-state) to reduce the heat effect generate by the DLP system. The above procedure was repeated with reconfigured array patterns for totally 16 times. As shown in Fig. 5(a), for imaging without any object, 16 measurements in a

#198504 - $15.00 USD Received 30 Sep 2013; accepted 5 Nov 2013; published 14 Nov 2013

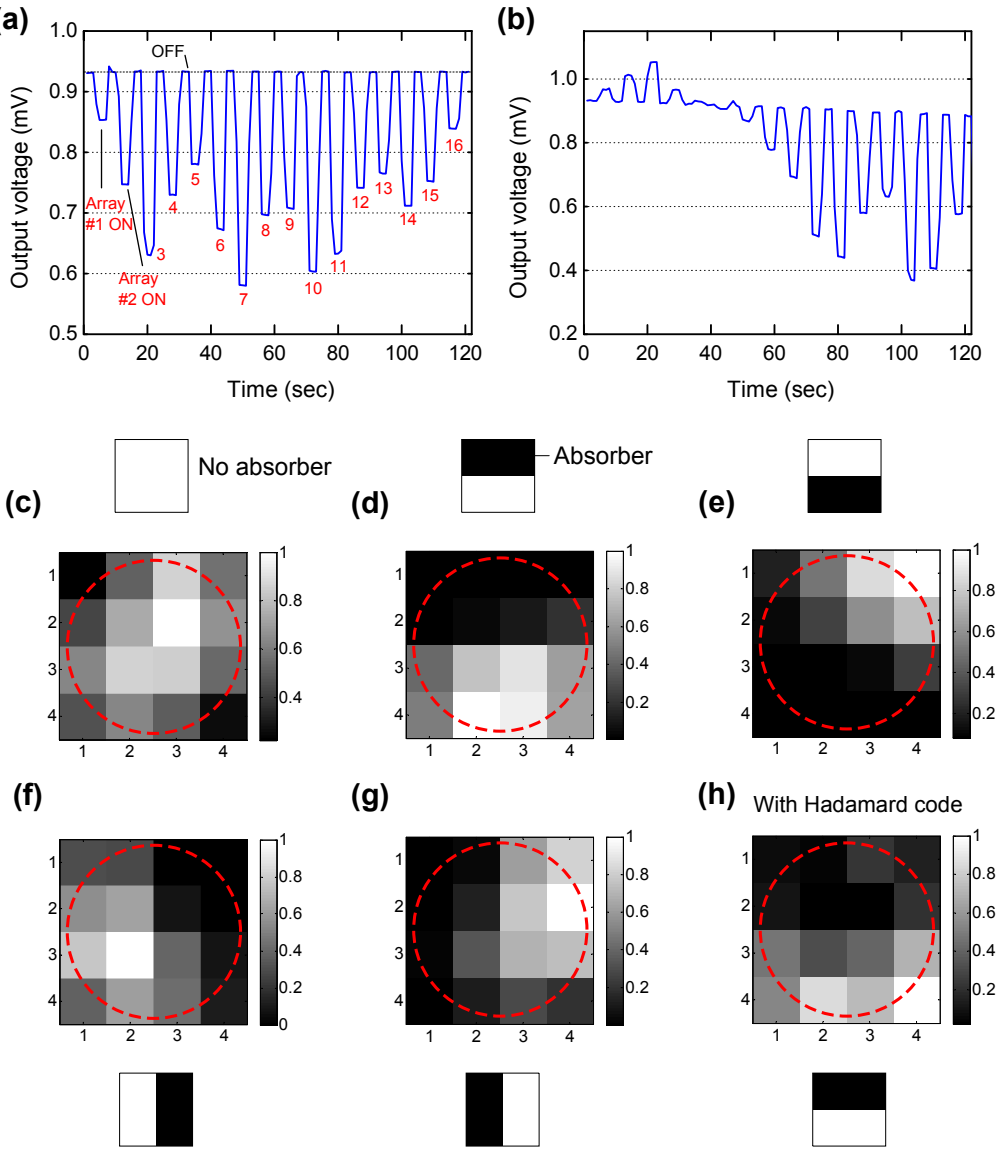

Fig. 5. 585 GHz 4 x 4 coded aperture imaging using photo-induced reconfigurable aperture arrays: (a) normalized measurement data without any object showing the imaging procedure, (b) normalized measurement data for object with upper-half of the imaging area blocked by an absorber, (c) reconstructed image from the measurement in (a) resolving the shape of THz beam presented as the bright region at the center (~8 mm beam size), (d) reconstructed image for upper-half block from the measurement in (b), (e)-(g) reconstructed image for lower-half block, left-half block and right-half block, respectively, and (h) imaging result for upper-half block using the well-known Hadamard coding [29]. The red dashed circles represent the THz beam cross-section.

duration of ~120 seconds were performed and the differences between each array ON and OFF states were taken as the image information for solving equations and reconstruction. In this relatively simple coding case, the image information for each measurement directly represents the relative THz intensity in that pixel. Figure 5(c) shows the image reconstructed from the data in Fig. 5(a). This image actually resolves the shape of the THz beam (~9 mm from calculation) at the position where the silicon wafer was placed. Although with relatively

#198504 - $15.00 USD Received 30 Sep 2013; accepted 5 Nov 2013; published 14 Nov 2013

low resolution, a bright region at the imaging area center (red dashed circles) is observed. To verify the effectiveness of this imaging approach, an absorber was used to block only the THz beam at the upper, lower, right and left half to form objects immediately adjacent to the silicon wafer. Figure 5(b) shows the data for upper-half block. It is clearly seen that pixels 1-8 became darker immediately implying much lower THz intensity at those pixels as displayed in the corresponding reconstructed image in Fig. 5(d). Figures 5(e)-5(g) show the reconstructed images for the rest objects and the results match the expectation quite well. In Fig. 5(h) shows an image for upper-half block using the well-known Hadamard coding [30] demonstrating similar imaging performance as compared to Fig. 5(d). For high-resolution CAI with many pixels, we expect that Hadamard coding should result in higher signal-to-noise ratio [30]. This imaging technique has been applied to map THz beams in a CW quasi-optical system and the corresponding results will be published elsewhere [32]. This approach may also find applications in quantum-cascade laser (QCL) optimization and characterization, as well as THz antenna characterization. Much improved imaging could be achieved by increasing the pixel numbers and adopting Haddmad coding or compressed coding [30, 31]. Finally, since the modulation speed of this technique was estimated to be ~1.3 KHz, a real-time video-rate (30 frame/s) imaging with 7 x 7 resolution can be potentially demonstrated. A room-temperature, real-time, compact and low-cost THz camera for many practical applications could be realized on the basis of this approach.

5. Conclusions

In conclusion, we present the capability and versatility of photo-induced THz modulation realized by illuminating reconfigurable patterns on silicon substrates using a commercially-available DLP system. By employing the proposed modulation technique, we have successfully demonstrated several modulation functions, including THz intensity modulation, tunable polarization and room-temperature coded-aperture imaging. We believe that real-time, low-cost and high-resolution THz cameras can be potentially developed by refining this technique with high performance THz detectors or receivers [15, 28] and specifically designed DLP chips/systems. The performance of THz modulation may be improved by using direct bandgap semiconductor such as GaAs due to its high quantum efficiency. Moreover, even with its high electron mobility, the short carrier lifetime in GaAs could significantly reduce the carrier diffusion length and therefore enhance the spatial resolution of photoinduced conducting patterns. Overall, we envision that this technique could be applied to realize a variety of cost-effective reconfigurable quasi-optical THz circuits and components such as universally tunable filters, planar tunable zone-plates and spatial arrays for much improved THz wave manipulation capability desired in THz imaging, sensing and communication.

Acknowledgments

The authors would like to thank Drs. P. Fay and H. Xing in the Department of Electrical Engineering, University of Notre Dame for valuable discussions. This work was partially supported by NSF Grants ECCS-1002088 and ECCS-1102214. The authors also would like to acknowledge partial supports from the Advanced Diagnostics and Therapeutics (AD&T) and the Center for Nano Science and Technology (NDnano) at the University of Notre Dame.

#198504 - $15.00 USD Received 30 Sep 2013; accepted 5 Nov 2013; published 14 Nov 2013